Fuel 364 (2024) 131096

Contents lists available at ScienceDirect

Fuel

journal homepage: www.elsevier.com/locate/fuel

Chemical reactor network modeling in the context of solid fuel combustion under oxy-fuel atmospheres

Sören Dübal [a], Leon L. Berkel [b], Paulo Debiagi [b,c], Hendrik Nicolai [b,*], Tiziano Faravelli [d], Christian Hasse [b], Sandra Hartl [a]

[a] Department of Mechanical and Plastics Engineering, University of Applied Sciences Darmstadt, Schöfferstraße 3, Darmstadt, 64295, Germany
[b] Simulation of Reactive Thermo-Fluid Systems, Technical University of Darmstadt, Otto-Berndt-Str. 2, Darmstadt, 64287, Germany
[c] Nottingham Ningbo China Beacons of Excellence Research and Innovation Institute, University of Nottingham Ningbo China, Ningbo, 315100, China
[d] Department of Chemistry, Materials and Chemical Engineering, Politecnico di Milano, Piazza Leonardo Da Vinci 32, Milan, 20133, Italy

ARTICLE INFO

Keywords:
Chemical reactor network
Pulverized solid fuel combustion
Detailed chemistry
Oxy-fuel combustion

ABSTRACT

A multi-phase chemical reactor network (CRN) is developed and applied to investigate solid fuel combustion under oxy-fuel atmospheres in a laboratory-scale combustion chamber. The development of a novel solid-gas plug flow reactor (sPFR) allows the full coupling of solid and gas phase processes to increase the fidelity in CRN modeling. Together with the recently developed solid-gas perfectly stirred reactor (sPSR), the new sPFR is applied within a multi-phase reactor network to model the complex features of the investigated application. To design an initial reactor network, a hybrid experimental and computational fluid dynamics (CFD)-driven approach is being pursued, taking into account both global and local information on flow and temperature fields. Initially, an in-depth investigation of the physical processes is conducted, covering solid fuel conversion processes such as devolatilization and char conversion, along with the thermochemical characteristics of the flue gas. In particular, the prediction of carbon monoxide (CO) emissions is analyzed in detail by means of sensitivity analyses. Based on the findings of the sensitivity study, the network complexity of the initial reactor network is increased to enable an accurate prediction of the CO formation in comparison to the experiments. Finally, the formation of nitric oxides (NOx), sulfur oxides (SOx), and aromatic pollutants is discussed, highlighting the importance of detailed chemistry in solid fuel combustion at technically relevant scales.

1. Introduction

Mitigating industrial emissions from power plants is highly relevant, particularly due to the significant contribution of hydrocarbon fuel combustion to CO_2 emissions [1]. Oxy-fuel combustion coupled with carbon capture and storage (CCS) presents a promising approach for achieving substantial reductions in CO_2 emissions from power plants. By replacing the atmospheric N_2 with CO_2 prior to combustion, the flue gas mainly consists of CO_2. However, substituting N_2 with CO_2 significantly affects the combustion process, due to the different physical properties of CO_2, such as a higher heat capacity [2].

To gain a profound understanding of combustion processes under oxy-fuel atmospheres, experimental studies were performed at various configurations, ranging from laboratory-scale combustion [3–5] to pilot-scale systems [6,7]. Moreover, recent numerical studies demonstrated that the main combustion characteristics and detailed flow behavior are consistent with experiments [8–10]. One major drawback for detailed CFD simulations for designing technical relevant plants is prohibitive computational costs associated with the multi-physics and multi-scale problem. In particular, the direct coupling of a detailed flow with physical and chemical processes during the pulverized coal combustion (PCC) process, including gas-phase reactions, devolatilization and heterogeneous char oxidation requires a large computational effort. To capture the complex chemistry considering solid and gas-phase reactions, simplified global kinetics are often used [8,11]. While these methods correctly capture global characteristics, the prediction of minor species, such as (CO), remains challenging [12].

As an alternative to CFD, scale-reduced modeling approaches have emerged. They present an efficient method to provide a precise prediction of pollutants also in complex systems [13–16]. Due to the low computational effort compared to CFD, they can present a path towards simulation aided-design of larger-scale combustion systems. Chemical reactor network (CRN) models allow the coupling of detailed chemical kinetics (comprising hundreds of species and tenthousands of reactions)

* Corresponding author.
E-mail address: nicolai@stfs-tu.darmstadt.de (H. Nicolai).

https://doi.org/10.1016/j.fuel.2024.131096
Received 10 November 2023; Received in revised form 22 January 2024; Accepted 25 January 2024
Available online 30 January 2024

to a simplified flow representation. By dividing complex systems into functional macro zones, so-called compartments [17,18], flow patterns can be represented by ideal reactor models [13].

The approach was initially applied on a pilot-scale furnace to predict nitrogen oxides [14,19,20]. The flow and temperature fields were taken from a CFD study with simplified chemistry. Using this data, Perfectly Stirred Reactors (PSR) were applied on zones larger than the CFD cells and calculated with detailed chemistry. In a recent study, Trespi et al. [13] demonstrated that the reactor network approach can predict CO emissions in single-phase oxy-fuel combustion. To represent the complex flow behavior more accurately, a reactor network consisting of PSRs and Plug Flow Reactors (PFR) for straight flow patterns with fully coupled recycle streams is considered. The CRN design is based on a hybrid approach [17] using experimental and CFD data.

Initial efforts have also been made to further develop CRN approaches for multi-phase applications [21–25]. Menage et al. [21] designed a CRN from CFD simulations of PCC for several pulverized coal jet flames in a flat flame reactor using PSRs. A global devolatilization scheme and a simplified representation of char oxidation, accounting for solid conversion, were coupled with a detailed gas-phase kinetic mechanism to examine devolatilization rates and concentration profiles of various gaseous species. Ishihara et al. [22] performed a CRN analysis for an industrial scale pulverized-coal fired burner to investigate the potential of ammonia co-firing. Focussing on the prediction of NOx emissions, they employed a detailed gas-phase mechanism coupled with simplified solid-gas reactions involving the reactions of NO with soot and char. In the context of biomass gasification in a fluidized bed reactor, a solid-gas perfectly stirred reactor unit (sPSR) was recently introduced by Berkel et al. [25]. This reactor type fully couples the gas and solid phase reactions. A reactor network that combines the multi-phase sPSR together with gas-phase PFRs using detailed descriptions of both gas-phase and solid-phase chemistry by the CRECK-S-B model [26], was designed to investigate biomass conversion.

As mentioned above, reactor network analyses in the context of solid fuel conversion have focused exclusively on coupled solid and gas reactions in PSR units. However, to better capture the fluid dynamics in compartments with a straight flow pattern, using a multi-phase plug-flow reactor unit is desirable. Therefore, this work introduces a solid-gas plug flow reactor (sPFR) model that enables the design of a complex reactor network. This development allows, for the first time, the application and assessment of multi-phase CRNs employing detailed chemistry on a laboratory-scale combustor with a complex flow field under oxy-fuel atmospheres.

The outline of this work is structured as follows. Section 2 first describes the basics of CRN modeling, followed by a detailed discussion of the new solid-gas plug flow reactor. Subsequently, the chemical modeling for solid fuel conversion is summarized. Section 3 presents the experimental configuration and numerical simulations enabling the hybrid approach. Section 4 discusses the results of the initial CRN, as well as sensitivity-based network designs. Finally, Section 5 summarizes the main findings of this work.

2. Modeling and numerics

Chemical reactor networks consist of several components. Ideal reactor models describe the chemical reactions in the respective functional zones. Generally, two types of reactors are employed to describe the characteristic flow behavior of the system. Regions with strong mixing, such as recirculation zones (RZ), are modeled with a PSR. The PFR model approximates straight flow patterns. Within a multi-phase CRN, streams contain gas and solid mass flows consisting of species that represent the respective phase. Further, auxiliary units for mixing and splitting the flow are required to connect and split streams originating from different units for the connection between reactors. Furthermore, recirculated flows can be taken into consideration such that a unit's input relies on its output, and a fully coupled solution must be calculated for this particular segment of the network. Fig. 1 gives an example of a generic CRN configuration.

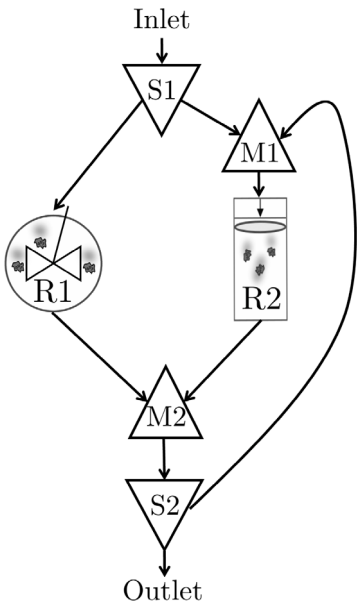

Fig. 1. Generic reactor network containing a sPSR (R1), the novel sPFR (R2) as well as mixing (M1) and splitting (S1) units.

Ideal mixing in multi-phase CRNs is already tackled with the sPSR model. The mass balance equations for the zero-dimensional reactor are formulated across the entire reactor volume as follows:

$$\frac{\mathrm{d}\dot{m}_{i,\mathrm{Gas}}}{\mathrm{d}t} = \dot{m}_{\mathrm{in,Gas}} \cdot Y_{i,\mathrm{in}} - \dot{m}_{\mathrm{in,Gas}} \cdot Y_{i,\mathrm{out}} + \dot{\omega}_i \cdot \mathrm{MW}_i \cdot V \qquad = 0 \quad (1)$$

$$\frac{\mathrm{d}\dot{m}_{j,\mathrm{Solid}}}{\mathrm{d}t} = \dot{m}_{\mathrm{in,Solid}} \cdot Y_{j,\mathrm{in}} - \dot{m}_{\mathrm{in,Solid}} \cdot Y_{j,\mathrm{out}} + \dot{\omega}_j \cdot \mathrm{MW}_j \cdot V \qquad = 0 \quad (2)$$

More information on the sPSR model can be found in [25].

2.1. Solid-gas plug flow reactor model

In PCC, both homogeneous and heterogeneous reactions take place simultaneously along directed flows. The solid-gas plug flow reactor (sPFR) enables the modeling of heterogeneous reactions important for solid fuel combustion. Following the idea of the plug flow reactor model, the sPFR model assumes no back-mixing in the flow direction, while simultaneously presuming perfect radial mixing. A fundamental aspect of the sPFR model is the direct coupling of the gas phase and the solid phase. This reactor design features a constant cross-sectional area that is shared by both phases. Similar to the solid-gas perfectly stirred reactor [25], following assumptions regarding the solid phase treatment are made:

- Gas and solid phases are perfectly mixed in the radial direction and occupy different volumes.
- Particles are treated on a volumetric basis. Transport effects between gas and solid are not explicitly modeled.
- Gas and solid phase have the same residence time and, therefore, equal velocities.
- The density of the solid phase remains constant, although the volume may change.

The thermodynamic state of the sPFR model is fully described by the pressure and the gas and solid phase temperatures and compositions. The solid composition is determined by the partial densities of the respective solid species, described in 2.2 in more detail. As a first step, it is assumed that the particles are completely entrained with the gas flow, resulting in the same residence time as the gas phase. Fig. 2

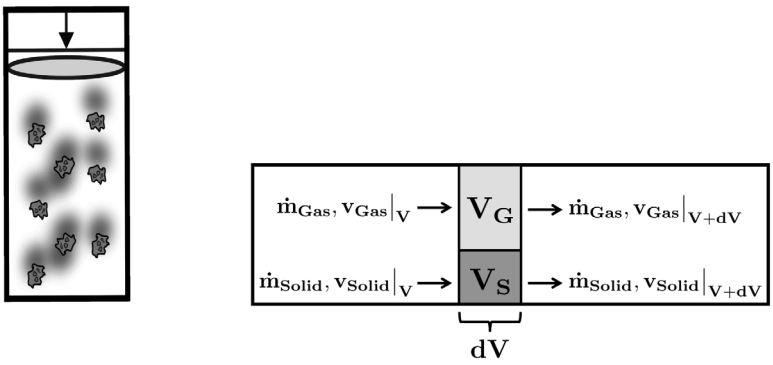

Fig. 2. Schematic depiction (left) and mathematical model of the solid-gas plug flow reactor model (right).

shows a schematic illustration and the mass balances of each phase at an infinitesimal volume element within the solid-gas plug flow reactor. Starting from the single-phase PFR, the model equations describe the mass flows $\dot{m}_{i,\mathrm{Gas}}$ of each component along an infinitesimal volume element $\mathrm{d}V$ in steady state conditions:

$$\frac{\mathrm{d}\dot{m}_{i,\mathrm{Gas}}}{\mathrm{d}V} = \dot{\omega}_i \cdot \mathrm{MW}_i \tag{3}$$

The mass balance equations for the gas and solid phase in the infinitesimal volume of the sPFR model are derived in a similar manner:

$$\dot{m}_{i,\mathrm{Gas}}\Big|_{\mathrm{V}} - \dot{m}_{i,\mathrm{Gas}}\Big|_{\mathrm{V+dV}} + \dot{\omega}_i\Big|_{\mathrm{V}} \cdot \mathrm{MW}_i \cdot \mathrm{d}V = 0 \tag{4}$$

$$\dot{m}_{j,\mathrm{Solid}}\Big|_{\mathrm{V}} - \dot{m}_{j,\mathrm{Solid}}\Big|_{\mathrm{V+dV}} + \dot{\omega}_j\Big|_{\mathrm{V}} \cdot \mathrm{MW}_j \cdot \mathrm{d}V = 0 \tag{5}$$

In Eqs. (4) and (5), $\dot{m}_{i,\mathrm{Gas}}$ and $\dot{m}_{j,\mathrm{Solid}}$ denote the mass flows of the gaseous and solid species. The formation rates $\dot{\omega}$ and the molecular weights MW take into account the change of mass flows due to chemical reactions. This formulation allows changing the masses of individual phases and conserving the total mass throughout the reactor. The formation rates of gaseous species depend on gas-phase reactions $\dot{\omega}_{i,\mathrm{Gas}}$, as well as reactions involving the solid phase $\dot{\omega}_{i,\mathrm{GasFromSolid}}$. On the other hand, only solid phase reactions contribute to the formation rates of solid species $\dot{\omega}_{j,\mathrm{Solid}}$. Hence, the species mass fractions along the reactor are given by:

$$\frac{\mathrm{d}Y_{i,\mathrm{Gas}}}{\mathrm{d}z} = A \cdot \frac{\mathrm{MW}_i}{\dot{m}_{\mathrm{Gas}}} \cdot \left(\alpha_{\mathrm{Gas}} \cdot \dot{\omega}_{i,\mathrm{Gas}} + \alpha_{\mathrm{Solid}} \cdot \dot{\omega}_{i,\mathrm{GasFromSolid}}\right) - \frac{Y_{i,\mathrm{Gas}}}{\dot{m}_{\mathrm{Gas}}} \cdot \frac{\mathrm{d}\dot{m}_{\mathrm{Gas}}}{\mathrm{d}z} \tag{6}$$

$$\frac{\mathrm{d}Y_{j,\mathrm{Solid}}}{\mathrm{d}z} = A \cdot \frac{\mathrm{MW}_j}{\dot{m}_{\mathrm{Solid}}} \cdot \left(\alpha_{\mathrm{Solid}} \cdot \dot{\omega}_{j,\mathrm{Solid}}\right) - \frac{Y_{j,\mathrm{Solid}}}{\dot{m}_{\mathrm{Solid}}} \cdot \frac{\mathrm{d}\dot{m}_{\mathrm{Solid}}}{\mathrm{d}z} \tag{7}$$

The area fractions α_{Gas} and α_{Solid} of the total volume $V = A \cdot \mathrm{d}z$, are introduced to distinguish between the two phases. Due to the constant cross-sectional area A of the solid-gas plug flow reactor, the volume fractions are equal to area fractions

$$\alpha_{\mathrm{Gas}} = \frac{A_{\mathrm{Gas}}}{A} = \frac{\frac{\dot{m}_{\mathrm{Gas}}}{\rho_{\mathrm{Gas}} \cdot v_{\mathrm{Gas}}}}{A} \tag{8}$$

$$\alpha_{\mathrm{Solid}} = \frac{A_{\mathrm{Solid}}}{A} = \frac{\frac{\dot{m}_{\mathrm{Solid}}}{\rho_{\mathrm{Solid}} \cdot v_{\mathrm{Solid}}}}{A}. \tag{9}$$

To solve Eqs. (6) and (7), further equations accounting for the change in the total mass flows of each phase are required.

$$\frac{\mathrm{d}\dot{m}_{\mathrm{Gas}}}{\mathrm{d}z} = A \cdot \dot{\omega}_{\mathrm{tot,GasFromSolid}} \cdot \alpha_{\mathrm{Solid}} \tag{10}$$

$$\frac{\mathrm{d}\dot{m}_{\mathrm{Solid}}}{\mathrm{d}z} = A \cdot \dot{\omega}_{\mathrm{tot,Solid}} \cdot \alpha_{\mathrm{Solid}} \tag{11}$$

The total formation rates $\dot{\omega}_{\mathrm{tot}}$ are obtained by summing up the formation rates of all species in each phase.

Table 1
Ultimate analysis of Rhenish lignite used in this study [29] and characterization of main reference coals in the CRECK-S model.

Ultimate analysis	(wt-%)	Reference coals	(wt-%)
Carbon	77.03	COAL1	0
Hydrogen	4.85	COAL2	58.39
Oxygen	16.80	COAL3	35.80
Nitrogen	0.98	CHAR-C	5.81
Sulfur	0.34		

2.2. Solid and gas phase kinetics

In order to calculate the conversion rates in the formation terms in e.g. Eq. (6), the seamless CRECK-S-C model for the thermochemical conversion of coal is employed. The kinetic mechanism in this work is based on Sommariva et al. [27], which was further validated for oxy-fuel conditions [28].

The underlying methodology of the CRECK-S model characterizes solids using a limited number of reference species that represent the main chemical structures in the coal [11]. A coal sample can be described by the linear combination of the reference species in order to satisfy the elemental mass balances. The Van Krevelen diagram in Fig. 3 shows the composition of the Rhenish lignite (RL) used in this study in relation to the respective reference species. Using triangulation, the Rhenish lignite is characterized by the monomers COAL-2, COAL-3 as well as CHAR-C. Table 1 reports the coals ultimate analysis and model characterization. More detailed information on the characterization of the solids within the CRECK-S model can be found in [11,27,28].

Each reference species has independent reaction pathways within the CRECK-S model. The reaction pathways take into account pyrolysis, char formation and the heterogeneous processes of char oxidation and gasification. The CRECK-S model calculates the heterogeneous reactions on a volumetric basis. To account for changing surface structures, as well as intra-pore diffusion, an effectiveness factor is applied to the metaplast and char oxidation reactions, for more information see [28,30]. Due to the detailed description of the gases released from the solids, the solid mechanism can be directly coupled with a detailed gas phase mechanism [28]. The complete kinetic mechanism applied in this work contains 192 gaseous and 42 solid species, encompassing around 2500 gas-phase reactions and 95 solid reactions.

2.3. CRN modeling

The newly developed sPFR model is implemented in the academic code NetSMOKE [13] within the scope of this work. The solver, which is based on OpenSMOKE++ [31] libraries, already utilizes model equations for single-phase reactors, such as the PFR and PSR, as well as the recently introduced sPSR. NetSMOKE has successfully been applied to single-phase combustion under oxy-fuel atmospheres [13] as well as the multi-phase gasification of biomass [25].

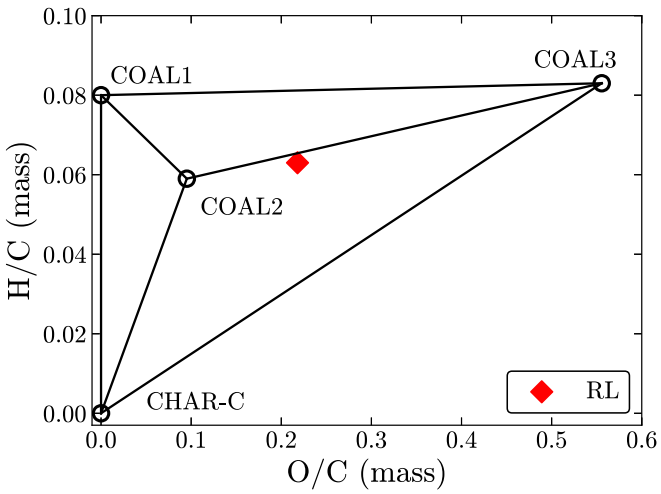

Fig. 3. Van Krevelen diagram depicting the location of CRECK-S reference species. The location of Rhenish Lignite (RL), the coal sample used in this study, is shown in red. *Source:* Adapted from [10].

The mathematical description of the entire reactor network results in a system of non-linear equations. If recycle streams occur, the input of affected units can depend on the output of downstream units and a global solution method has to be employed. Therefore, different solution algorithms are implemented to meet the desired computational and numerical requirements. Partitioning and sorting algorithms from the Boost Graph Library (BGL) [32] divide the network into strongly connected components (SCC) by identifying tear streams and an appropriate order for solving units within a SCC. With the sequential modular (SM) approach, each unit is solved in a given order from the inlet to the outlet of the respective SCC. A fully-coupled solution is obtained with an equation-oriented (EO) approach. In this study, the SCCs are solved employing both an SM approach and subsequently a fully-coupled approach to ensure overall convergence. For more details about the NetSMOKE algorithm, see [13,31].

3. Darmstadt laboratory-scale combustion chamber

Fig. 4 depicts the Darmstadt laboratory-scale combustion chamber. Pure gas flames and gas-assisted solid fuel flames, are investigated under air and oxy-fuel conditions. The combustion chamber has a cross section of 420 × 420 mm^2 with a height of 600 mm and operates under ambient pressures. Three inlets enter the combustion chamber from the top. The primary flow consists of a methane-oxidizer mixture and carries the pulverized solid fuel into the combustion chamber. The secondary flow provides additional oxidizer and enters through inclined channels leading to a swirled flow facilitating flame stabilization. A tertiary flow is added at the top of the combustion chamber to provide additional oxidizer for the char reactions [8,34]. The flue gases, together with solid residues, exit the combustor through an annular orifice. Due to the reduced length of the combustion chamber, incomplete particle burnout is to be expected.

Optical accessibility of the chamber body allows for optical diagnostics. Tunable diode laser absorption spectroscopy (TDLAS) measurements were carried out to investigate the thermochemical state of the flue gas, providing molar concentrations of major gas species, namely CO_2, H_2O, and CO as a pollutant [35]. Moreover, global residence time distributions (RTD) were measured by injecting an inert, gaseous tracer into the primary flow and measuring the time-resolved concentration at the outlet. It is assumed that the coal particles are entrained with the gas flow and therefore have similar residence times [34]. The RTD provides a global description of the flow inside the system under consideration [18].

In addition to the variety of experimental data, detailed LES studies have been carried out [8,29]. Here, solid fuel particles were modeled in an Euler-Lagrangian approach. The flamelet-based tabulation approach was employed to take into account detailed gas-phase kinetics within the LES. To describe solid fuel combustion, simplified models for the devolatilization and char reactions were employed. The flow and temperature fields of the LES study are consistent with insights from the experiments [8]. Thus the available data from CFD and experiments can be used in a hybrid approach to construct a corresponding CRN.

In combination with an assisting 20 kW methane flame, RL is combusted under oxy-fuel conditions consisting of 30 vol.-% O_2 and 70 vol.-% CO_2, resulting in a combined thermal output of 40 kW. These operating conditions will be referred to as RL30. Table 2 reports the mass flows and inlet compositions for the RL30 operation point. More specific information about the operating points is available in [8,35].

4. Results

The solid-gas plug flow reactor and the solid-gas perfectly stirred reactor are applied in a chemical reactor network model for the gas-assisted swirl combustor. Starting from the manual design process of the multi-phase CRN based on experimental and CFD data, the

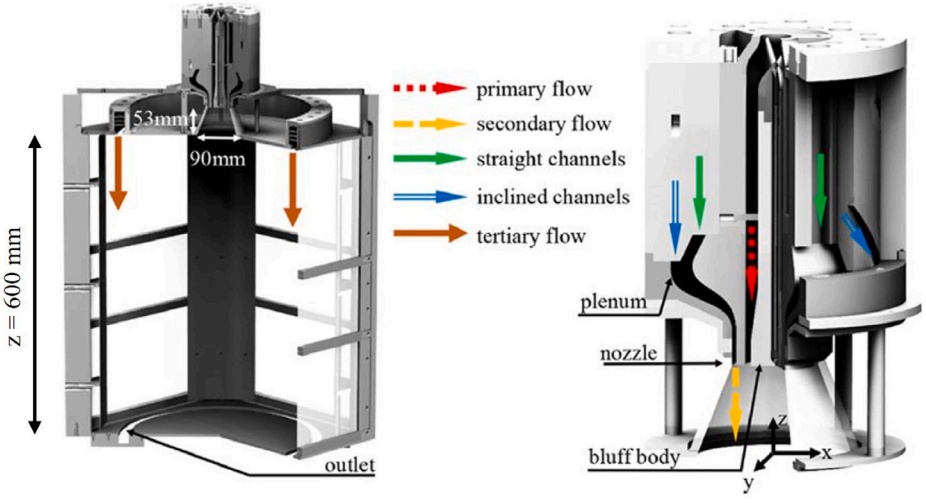

Fig. 4. Experimental configuration of the solid fuel combustion chamber [33].

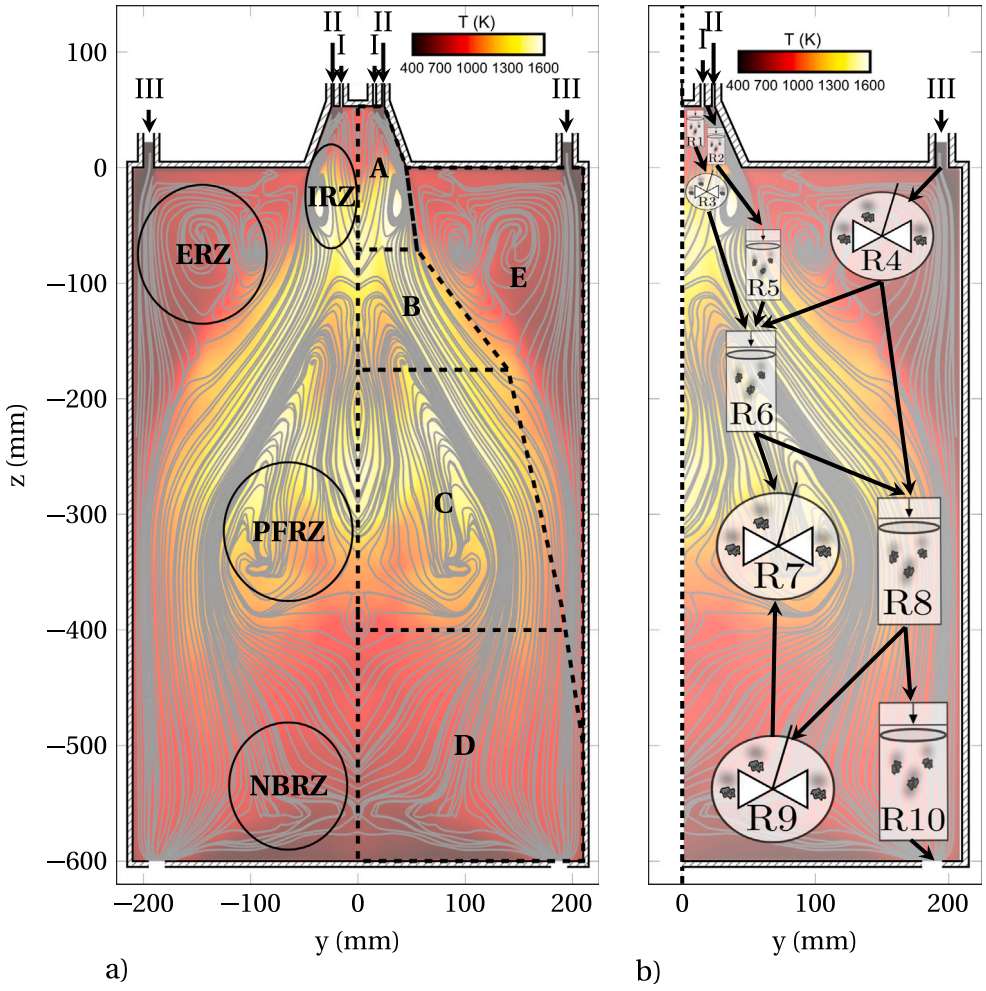

Fig. 5. Flow and temperature fields from CFD: (a) Identified recirculation zones and compartments of the combustor.(b) Simplified representation of the first chemical reactor network model (RN1) based on Trespi et al. [13]. For the sake of simplicity, the mixer and splitter units are not explicitly shown.

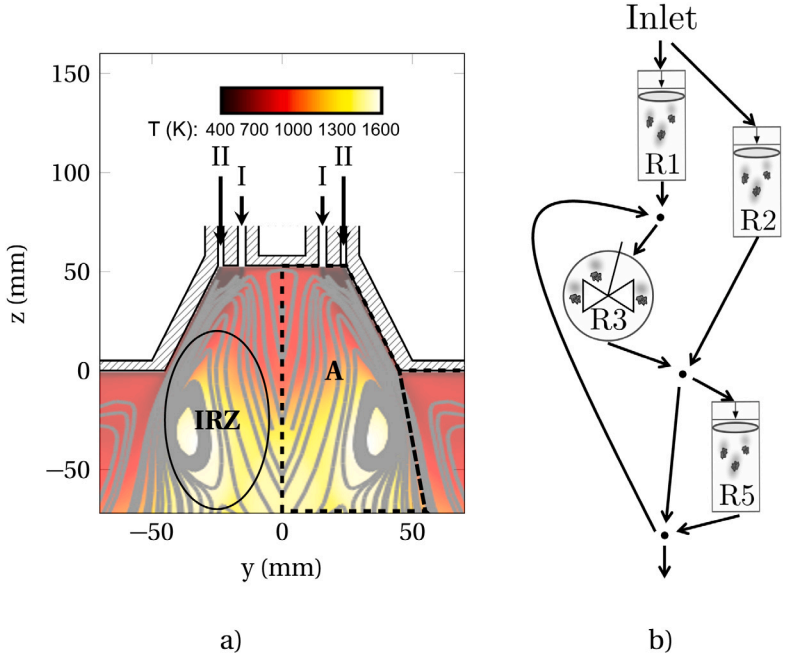

Fig. 6. Quarl region and inner recirculation zone from CFD (a) and the corresponding representation within the reactor network (b).

Table 2
Inlet composition and mass flow for the RL30 operating point.

	$\dot{m}_{gas}$ (kg s^{-1})	$\dot{m}_{solid}$ (kg s^{-1})	Y_{CH_4} (–)	Y_{O_2} (–)	Y_{CO_2} (–)
Primary flow	3.85×10^{-3}	9.28×10^{-4}	0.105	0.213	0.682
Secondary flow	5.56×10^{-3}	–	0.000	0.238	0.762
Tertiary flow	2.15×10^{-2}	–	0.000	0.238	0.762

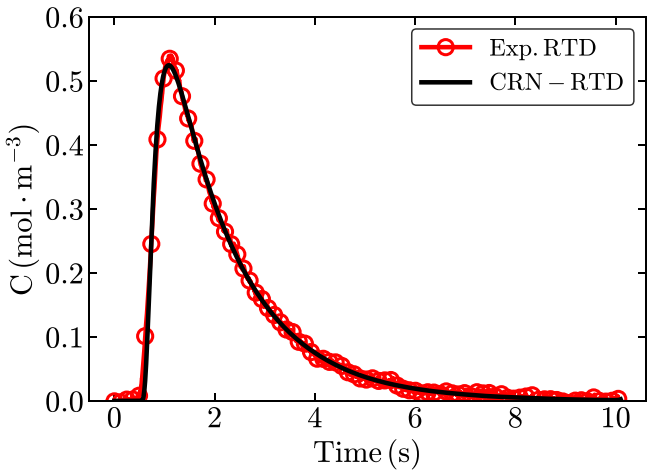

Fig. 7. RTD of the CRN obtained by the optimization procedure (black) compared to the experimental curve (red).

potentials and challenges of the approach are discussed. The prediction of major gaseous species and the sensitivity-based design targeting CO emissions are presented and discussed afterward. Finally, the advantages of detailed chemistry within the reactor networks will be emphasized through an analysis of different pollutants.

4.1. Initial reactor network design

Following Trespi et al. [13], the detailed description of the flow and temperature fields is used to identify macro zones to divide the complex combustor volume into functional compartments. As highlighted in Fig. 5(a), distinct recirculation zones can be identified inside of the combustor. The main flow characteristics of the multi-phase operating condition are similar to the single-phase operating condition [8,13]. Besides the characteristic inner recirculation zone (IRZ), marked as A in Fig. 5(a), three other recirculation zones can be detected in the combustor. Compartment E represents the external recirculation zone (ERZ), which arises from the tertiary flow. Further downstream, the post-flame recirculation zone (PFRZ) and the near-bottom recirculation zone (NBRZ) intensify further mixing of exhaust gases and partially burned-out particles. In Fig. 5(a), these compartments are labeled as C and D.

sPSRs approximate recirculation zones within the multi-phase CRN. The remaining volumes with directional streamlines, e.g. in compartment B, are modeled with the newly developed sPFR. Based on the trajectory of streamlines, the boundaries of compartments are approximated. In general, it has to be ensured that the sum of compartmental volumes is equal to the total volume of the modeled combustor. Following the first division of compartments considering the flow field, additional information on the temperature field is incorporated to set the reactor temperatures. Since the reactor temperature plays an important role in predicting the chemical conversion within a compartment correctly, compartments are further divided in case of large temperature variations. Fig. 5(b) depicts the simplified structure of the initial multi-phase CRN (RN1). The high-temperature regions of plug flow located downstream of the IRZ and adjacent to the ERZ emphasize

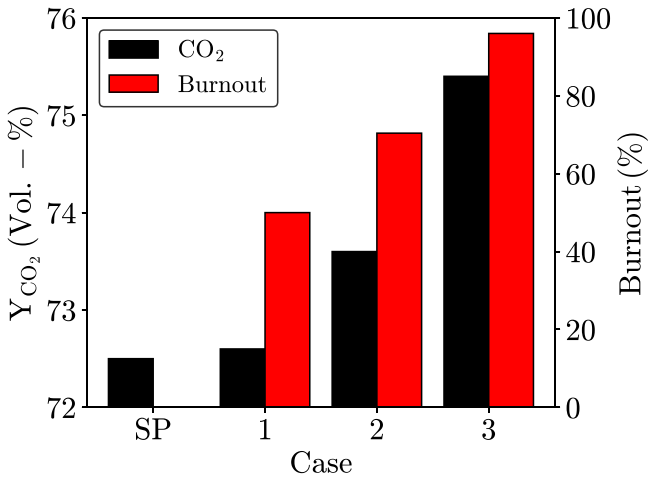

Fig. 8. CO_2 and Burnout determined with three different solid temperatures in the respective reactor network compared to single-phase CRN (SP) from Trespi et al. [13]. 1: CRN with solid temperatures from CFD. 2: RN1. 3: CRN close to complete burnout.

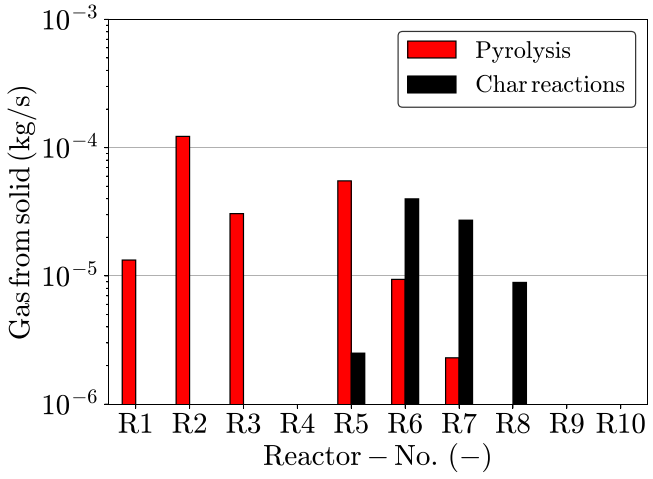

Fig. 9. Gas from solid particles due to Pyrolysis and Char Reactions in each reactor of RN1.

the need of an accurate representation in the reactor network that considers the flow entrained with solid particles in these areas.

Further attention needs to be directed to the modeling of the quarl and the IRZ. Complex physical processes, such as the heat-up of solid particles and the associated devolatilization primarily occur in these regions of the combustor. The particle size strongly affects the heating rates [8]. It is important to note that the solid phase is modeled as one single volume within the solid-gas reactors. Applying temperature profiles on sPFR units allows for a more accurate representation of the particle's heat up in straight flows. Fig. 6 provides an enlarged view of the quarl and the IRZ from CFD and their corresponding representation within the CRN. In addition to the previously introduced solid-gas reactor models, auxiliary units in the form of nodes are incorporated to represent mixing and splitting. The primary and secondary streams enter through the quarl. Due to the swirled secondary flow, the characteristic IRZ is formed. A notable portion of the flow bypasses the highly mixed zone, as shown by the streamlines. Hence, especially smaller particles are dragged towards the walls, instead of passing the IRZ initially. The inlet flow is divided and directed through two separate sPFRs within the CRN. The reactor R2 accounts for the bypass flow, whereas R1 directs a part of the inlet flow into the IRZ (R3). The resulting mixture from the bypass flow and the recirculation zone is

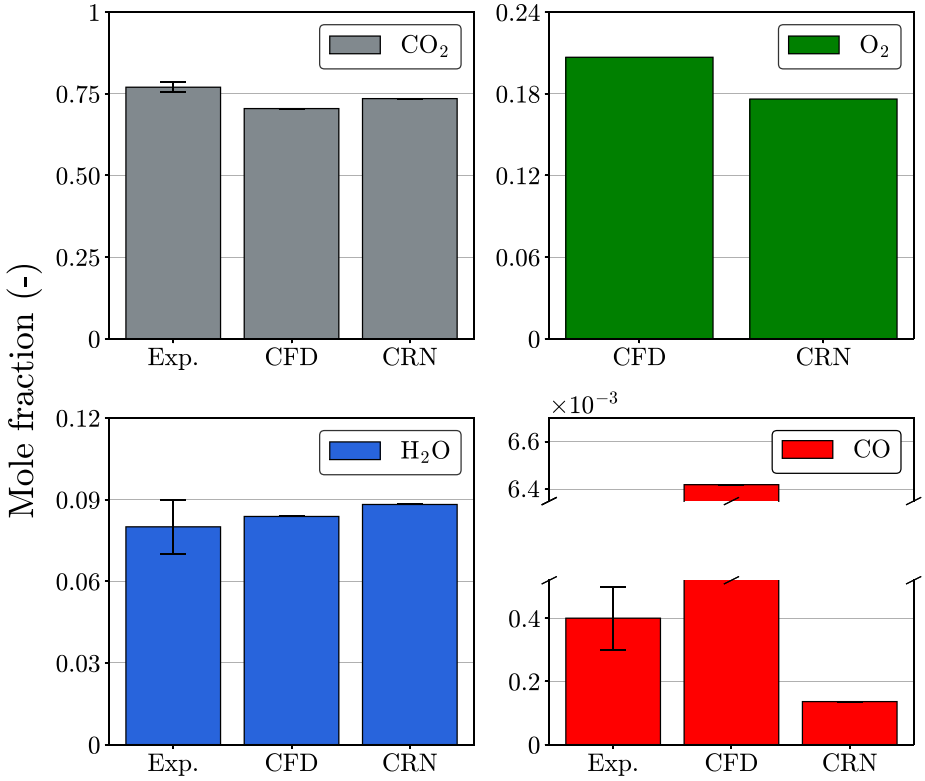

Fig. 10. Major species at the outlet of the CRN compared to results from the experiments [35] and CFD [8].

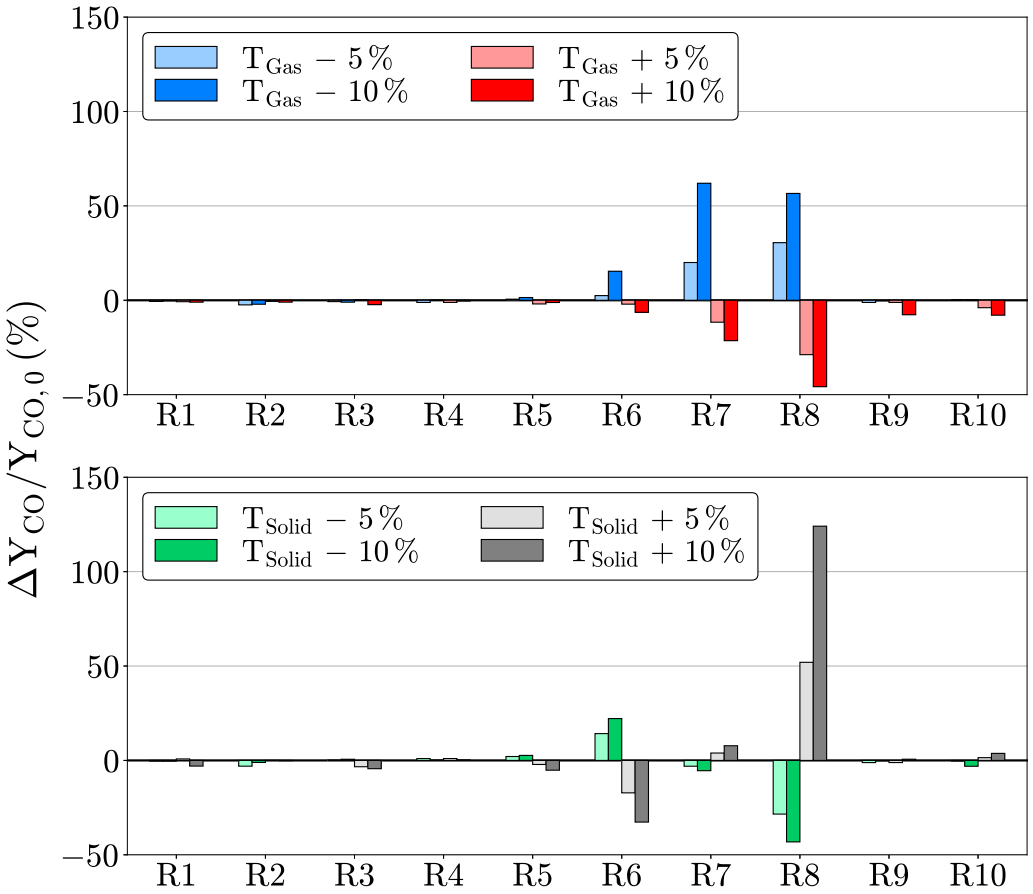

Fig. 11. Sensitivity studies with respect to gas and solid temperature variations of ±5/10% in each reactor and their impact on CO emissions at the outlet of RN1. Top: Variations in gas temperatures. Bottom: Variations in solid temperatures.

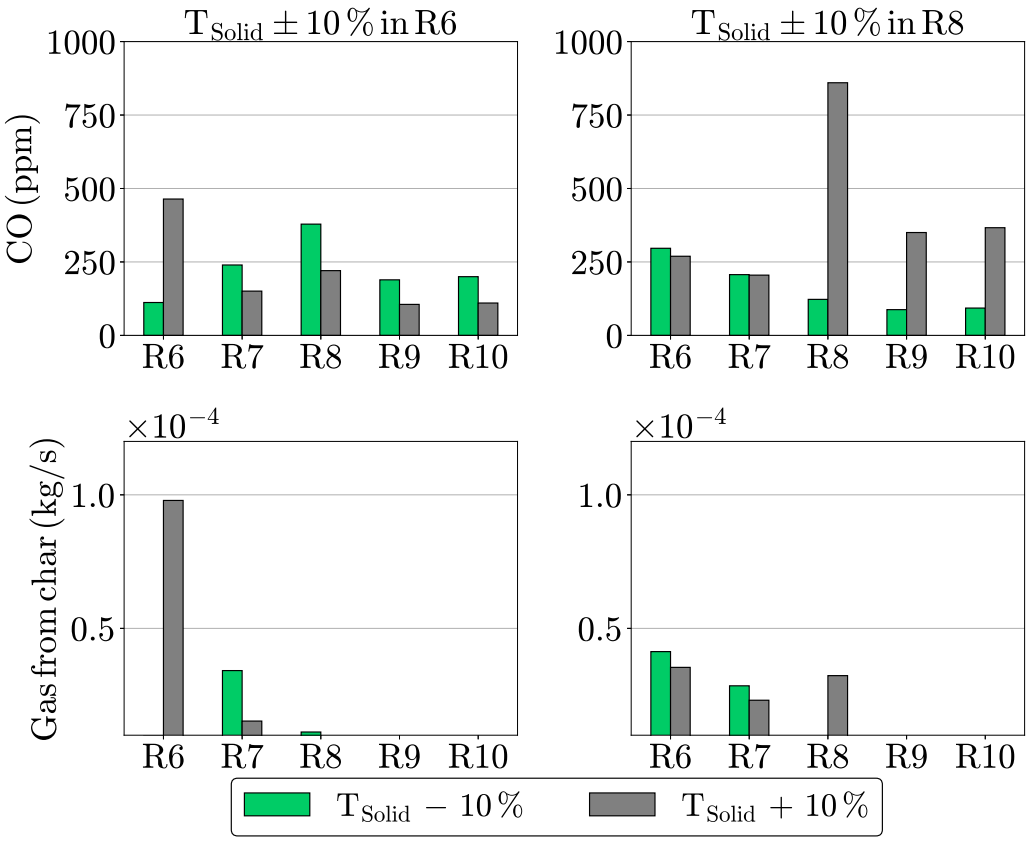

Fig. 12. Further analyses of the sensitivity studies considering R6 and R8 with respect to solid temperature variations of ±10%: CO concentrations (Top) and Char gases (Bottom) at the outlets of each reactor downstream from R6 through R10.

mixed. Subsequently, it enters another sPFR (R5) and is partly recycled back into the IRZ.

During the gas-assisted combustion of the lignite, the local temperatures vary between the two respective phases. After entering the quarl the gases heat up rapidly, reaching a maximum of approximately 1600 K around the IRZ and cooling down afterward. The solid phase exhibits a slower heating process and reaches its highest temperature further downstream, leading to a shift of the reaction zone compared to the single phase operation, as discussed in detail in previous works [8,13]. Due to the differences in gas and solid temperatures, a separate definition of temperatures for the respective phases is expected to improve prediction compared to defining a single temperature for both phases in one reactor. The solid temperature profile was derived from CFD data [8].

To capture the global flow behavior within the CRN [18], it is ensured that the CRN has the same RTD as the experimental reference. The RTD of the CRN is determined by the residence times of the individual reactors. Assuming a fixed reactor volume, the residence times depend on the flow splitting ratios inside the network, which represent a free parameter in the system. The splitting ratios are optimized to minimize the difference of RTD obtained from the network and experiment [36]. Therefore, the RTDs of the solid and gaseous phases are assumed to be equal, according to experiments [34]. The CRN calculation is included within the optimization routine to account for changes in gas mass flows due to heterogeneous reactions. Fig. 7 illustrates the experimental RTD and the optimized RTD of the reactor network. The experimental curve can be matched with the optimization routine, ensuring an accurate representation of the global flow characteristics with the CRN.

4.2. Particle conversion and flue gas composition

Accurately capturing the solid burnout within the CRN is of primary interest since the progress of coal conversion directly influences the composition of the major gaseous species as well as the thermal output in the real application. Since the solid kinetics are modeled using Arrhenius-type rate constants, the solid temperature is the critical parameter for solid conversion. The profile from CFD represents an average temperature profile over many different particle sizes, which are not considered within the CRN. Since the average profile is mass based, larger particles are overrepresented. Due to the slower heat up of the larger particles, the average solid temperatures in the upper portion of the reactor do not represent the heat up of smaller particles accurately. Therefore, three CRN simulations with different solid temperatures have been carried out to determine a reasonable burnout for this configuration.

Fig. 8 depicts the CO_2 concentrations and the burnout rates of the three cases. In addition, the results of the single-phase CRN, referred to as SP, reported by Trespi et al. [13], are depicted to provide a comparison with CO_2 emissions in the absence of burnout. Case 1 represents RN1 with solid temperatures assigned from the mass based average CFD profile. The solid temperatures of reactors located in the upper part of the combustor in Case 2 are chosen higher compared to Case 1 to accurately represent solid conversion, especially devolatilization, in these regions. In Case 3, the highest solid temperatures are assigned, leading to a nearly complete burnout of the coal particles. A direct correlation between the burnout and CO_2 emissions is evident. The burnout estimated in Case 1 is approximately 50%, almost entirely due to the release of volatiles and hardly any char conversion. Therefore, similar CO_2 concentrations are observed compared to the single-phase

operating point. The total burnout of RL determined in Case 2 is about 70%. Incomplete burnout is plausible due to the length of the combustion chamber, which leads to short residence times that are insufficient for complete char conversion. For further analysis of RN1, the solid temperatures from Case 2 are used throughout the rest of the study.

Within the reactor networks, the amount of volatiles and char gases in each reactor can be estimated. For this purpose, the sum of gas species formation rates from the corresponding pyrolysis and char reactions, as calculated within the CRECK-S model, are evaluated. Thus, the resulting mass flow of the gases that is released by the solids into the gas phase can be calculated via the reactor volume. Fig. 9 shows the amount of gases released by the coal due to pyrolysis (red) and char reactions (black) in each reactor of the considered CRN.

A clear separation between devolatilization and char burnout is noticeable. As previously mentioned, it is known from CFD that a large share of particles first follows the flow towards the wall and bypasses the recirculation zone. Thus, fresh particles enter reactor R2 and experience a rapid heat-up due to the high temperatures in the IRZ. The high heating rates lead to a significant devolatilization in the quarl region, which is consistent with the reference LES [8]. While the pyrolysis is finished, the char conversion is still incomplete. The slower char reactions occur further downstream, mostly in reactors R6, R7 and R8. The CRECK-S model facilitates the parallel description of pyrolysis and char conversion reactions and their contribution to CO production in e.g. R6. Due to the lower temperatures in this area, only marginal char conversion occurs in the reactors located near the outlet of the combustion chamber. Since the laboratory-scale combustor has been specially designed for optical access, lower temperatures are present in its lower portion.

Fig. 10 shows the composition of major species and CO from RN1 compared to experimental data [35] and LES [8] at the outlet of the combustion chamber. The oxygen mole fraction and local gas concentrations are not available from measurements; further information can be found in [35]. The measurement of local gas concentrations from non-intrusive, state-of-the-art measurements remain challenging in comparable multi-phase systems as can be seen in e.g. [7,37]. In general, the major species can be predicted satisfactorily with the multi-phase CRN, also considering the uncertainties from experiments [35]. Compared to the single phase operating condition [38] considering a 20 kW methane flame only, the flue gas contains higher mole fractions of CO_2 and H_2O. This contribution of the solid fuel to the thermo-chemical state of the exhaust gas can be reproduced by the CRN. Compared to CFD, RN1 predicts the CO mole fraction more accurately, highlighting the importance of detailed kinetics for predicting pollutant formation. However, CO formation is still underpredicted compared to the experiments, which will be further investigated next.

Trespi et al. [13] demonstrated that an increased network complexity leads to a better prediction of species due to better resolving temperature variations. For instance, the macro zones C (R6) and D (R8) in Fig. 5 with large temperature variations are modeled as single sPFRs. Since the reactors are isothermal, a constant velocity profile and an average temperature for the entire region are assumed. Hence, the strong temperature variations, which influence the formation and consumption of minor species, are not captured sufficiently. In addition, under- or over-predicting particle conversion by specifying inaccurate temperatures could significantly affect the CO in the gas-phase.

4.3. Sensitivity-based network improvements

To improve predictions of CO, the impact of local reactor temperatures as a source of uncertainty within the CRN, affecting the gas-phase chemistry and particle conversion, is further investigated. Therefore, sensitivity studies with respect to an increase and decrease in the gas and solid temperatures on CO emissions are carried out. The gas phase and solid temperatures are varied by ±5% and ±10% in each reactor,

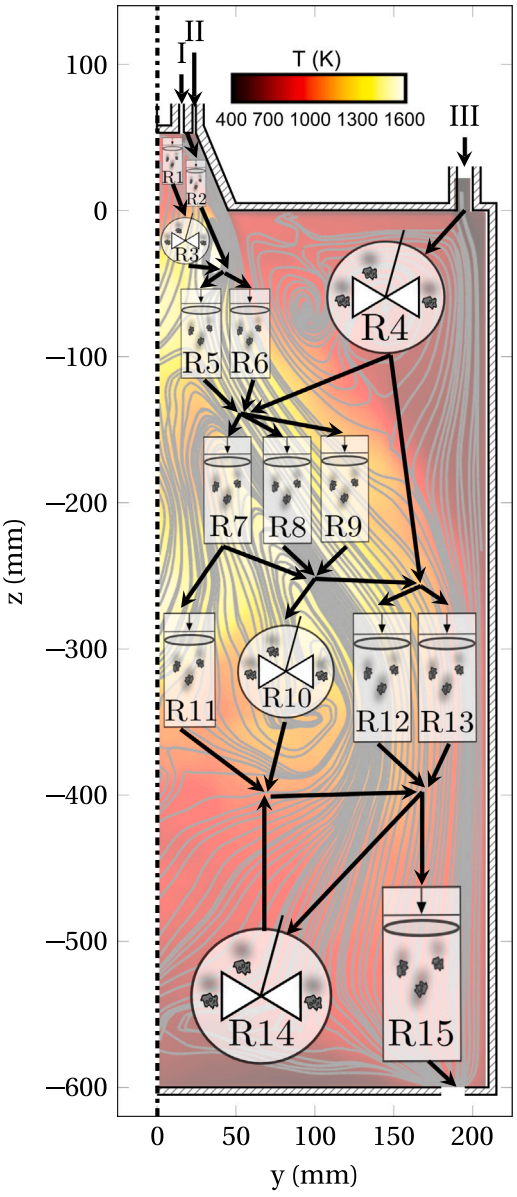

Fig. 13. Simplified representation of the improved CRN (RN2) based on findings of the sensitivity analyses.

respectively. The impact of the temperature variation is assessed by comparing the change in CO emissions of the corresponding CRN with the reference case RN1.

Fig. 11 depicts the results of the sensitivity study with respect to gas temperatures (top) and solid temperatures (bottom), respectively. In general, CO emissions are sensitive to temperature changes in both phases. A nonlinear behavior of CO emissions for temperature variations from 5 to 10 percent is evident, particularly in reactor R8. The temperature changes of the reactors around the PFRZ, represented by compartment C in Fig. 5(a), indicate a high sensitivity. In particular, the gas phase temperatures in reactors R7 and R8 prove to be critical for the CO emissions at the exit of the combustion chamber. Significant temperature variations occur in the gas phase in the region surrounding the PFRZ. As depicted in Fig. 9, char conversion mainly takes place in reactors R6, R7, and R8, resulting in CO formation. Here, lower gas phase temperatures result in reduced CO consumption, as evidenced by the increased CO emissions at the outlet. Conversely, higher gas temperatures lead to increased CO consumption. For the

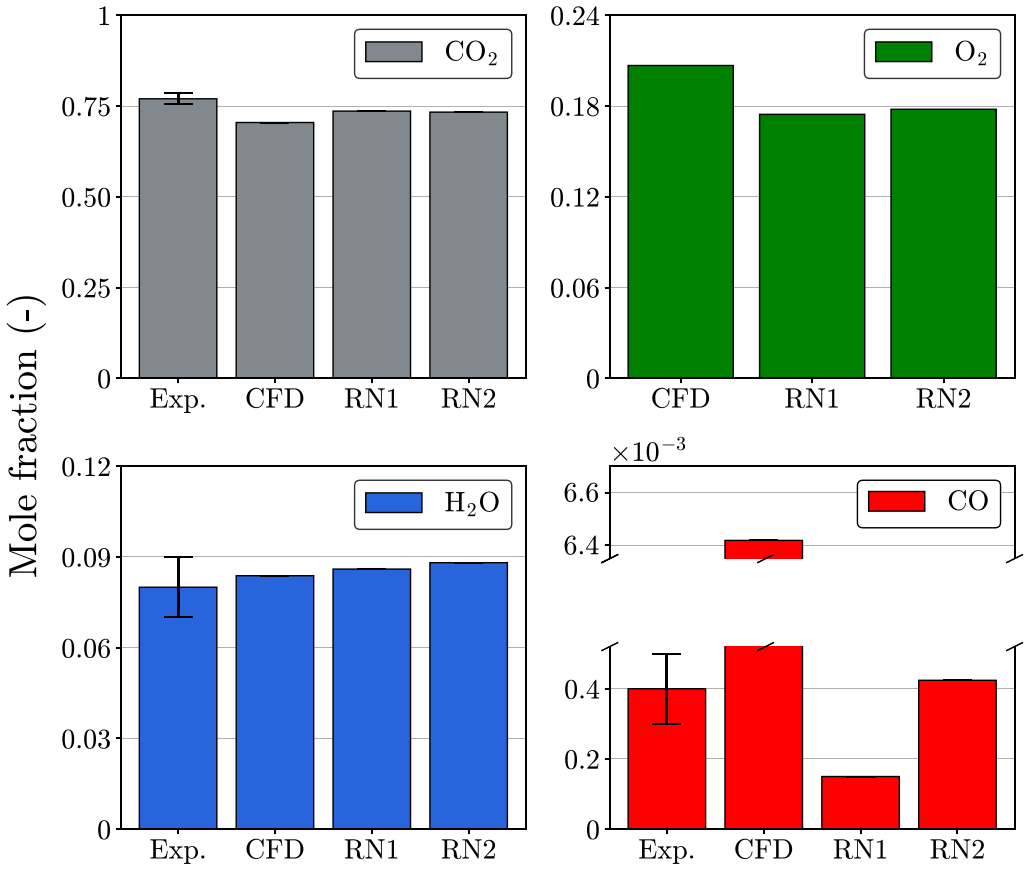

Fig. 14. Major species at the outlet of the RN2 compared to results from RN1, experiments [35] and CFD [8].

solid temperature variations, the reactor with the highest sensitivity to a temperature change is again R8. A contrasting trend is noticeable regarding the temperature variations in reactors R6 and R8. While the CO emissions at the outlet of the CRN decrease in the case of an increased temperature in R6, higher CO emissions are evident in the case of a temperature increase in R8.

This distinct behavior will be analyzed further, by examining the sensitivity studies regarding solid temperature variations of ±10% in R6 and R8 in more detail. Fig. 12 displays the concentrations of CO and the amount of char gases in each reactor downstream of R6. The particle conversion directly influences the CO concentration in the respective reactor, explaining the varying CO concentrations through the variation of solid temperatures. At an elevated solid temperature in R6, the largest amount of char is already converted in R6, which is reflected in the increased CO concentrations. Further downstream negligible conversion occurs, resulting in a marginal amount of CO from the solid conversion. Simultaneously, CO is consumed further due to gas phase reactions. For decreased solid temperatures in R6, there is reduced conversion in that reactor. The unconverted solid is then predominantly converted in R7 and R8. As a result, CO is released later and consumed less in the gas phase. The CO generated in R8 reacts only marginally in R9 and R10 due to the low gas-phase temperatures, leading to an increased CO concentration at the outlet of the combustion chamber. This behavior also explains the higher CO concentrations in case of an increased solid temperature in R8.

A refinement of the CRN based on the sensitivities is performed to better resolve temperature variations within the reactor network. The network complexity is increased by further refining regions, where single reactors exhibit the highest sensitivities with respect to gas-phase temperatures. Compared to RN1, these areas are modeled with additional solid-gas plug flow reactors (R6, R8, R9, R11, R13) to capture the effects of varying temperatures on CO formation. Fig. 13 illustrates the modifications, resulting in a new reactor network (RN2). Since a higher number of reactors and more auxiliary units are used for mixing and splitting, the processes inside the combustion chamber can be represented more accurately. Again, the splitting ratios are optimized to resemble the global flow behavior from the experiments. The optimized RTD curve for RN2 closely corresponds with the experimental RTD curve, similar to RN1. For the sake of brevity, the optimized curve is not displayed.

Fig. 14 shows the results for the optimized RN2. The more complex RN2 matches the experimental CO concentration in the flue gas accurately, compared to RN1 and the CFD. The better resolution of gas-phase temperature variations in the vicinity of the reaction zone increases the predictivity regarding CO emissions. For the solid phase, char conversion is now distributed over a larger share of reactors. On the other hand, small changes in the major species can be observed. These differences can be attributed to a slightly lower burnout compared to RN1, resulting in marginally lower CO_2 concentrations and more oxygen left at the outlet of the chamber. This approach demonstrates how a sensitive-based approach can improve CO predictions without significantly increasing the computational effort. Hence, a further increase of network complexity is not envisaged, especially since RN2 is able to accurately predict CO emissions.

Overall, the sensitivity studies reveal the reactors crucial to CO formation and consumption. Especially in regions approximated with plug flow reactors, the release of CO from char gases and its subsequent conversion in the gas phase have a significant impact on the overall CO emissions of reactor networks with varying degrees of complexity.

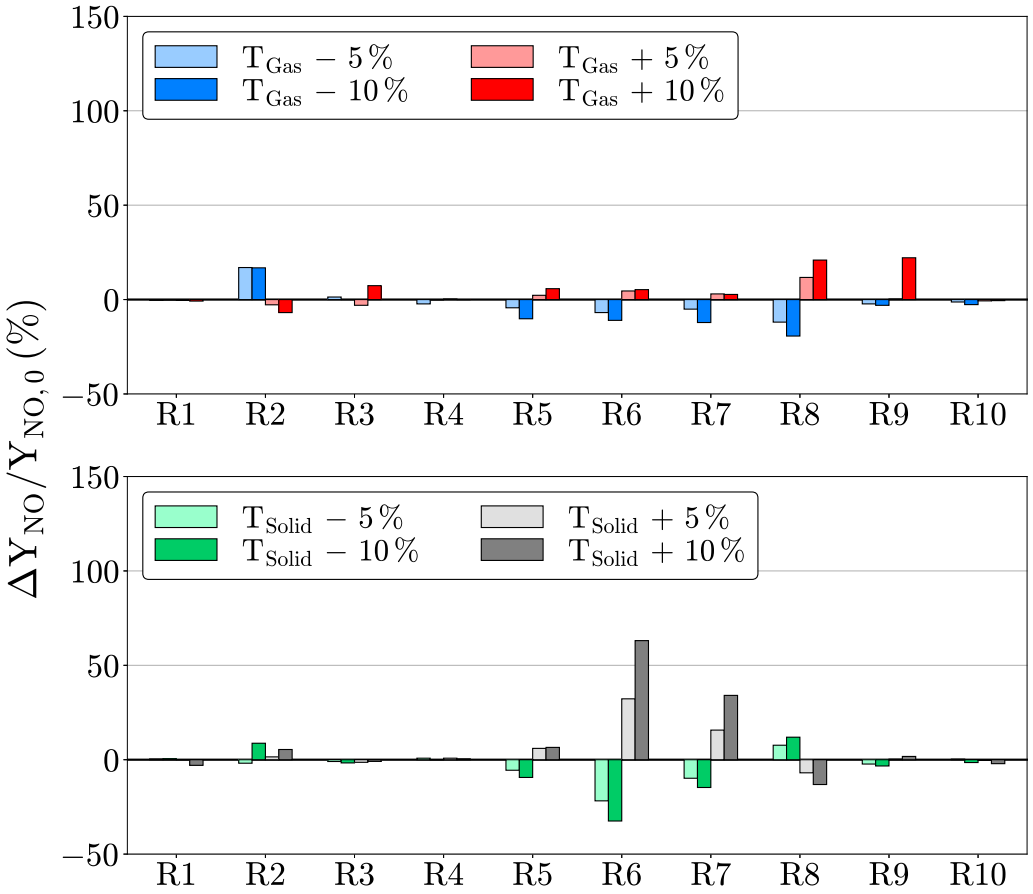

Fig. 15. Sensitivity studies with respect to gas and solid temperature variations of ±5/10% in each reactor and their impact on NO emissions at the outlet of RN1. Top: Variations in gas temperatures. Bottom: Variations in solid temperatures.

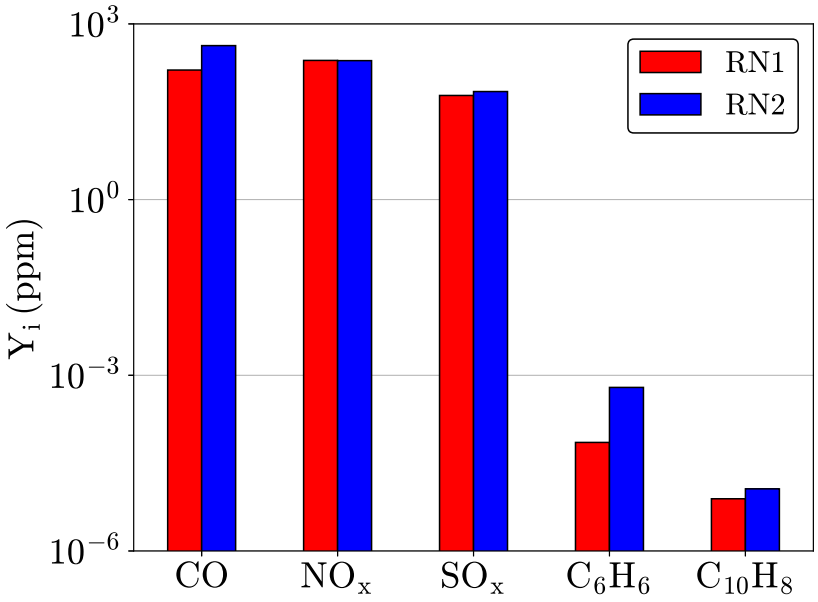

Fig. 16. Concentrations of selected pollutants at the outlet of RN1 and RN2.

4.4. Further pollutant analysis

After determining the residence times and temperatures of reactors based on CO emissions, the use of detailed kinetic mechanisms in reactor networks enables the prediction of other relevant minor species. Further common pollutants found in coal combustion, such as nitric oxides (NOx), sulfur oxides (SOx), and aromatic components are investigated in the following.

The primary source of NO in coal combustion is fuel-bound nitrogen, particularly in oxy-fuel combustion, while thermal and prompt NO play a minor role due to lower partial pressure of N2 and lower temperatures (<1800 K) [2,39,40]. Fig. 15 depicts the results of the

sensitivity analysis of RN1 to investigate NO formation within the multi-phase CRN. Lower sensitivities to temperature variations are generally observed in both phases, compared to CO. As anticipated, there are only minor sensitivities to gas phase temperatures and considerably higher sensitivities to solid temperatures. In the CRECK-S model, NO is formed from volatiles such as NH_3 or HCN and the oxidation of nitrogen present in char. Solid temperature variations in the reactors that represent the reaction zone, as with CO formation, are crucial to NO formation.

To provide an overview of minor species prediction, Fig. 16 presents a comparison of selected pollutants at the outlets of RN1 and RN2. When compared to CO, concentrations of NOx and SOx are within the same order of magnitude and are hardly affected by the increasing network complexity. Aromatic components, represented by benzene (C_6H_6) and naphthalene ($C_{10}H_8$) are below the parts per billion range and could be further coupled to advanced models to predict soot formation.

5. Conclusions

A multi-phase reactor network was developed and applied to a laboratory-scale combustor in the context of solid oxy-fuel combustion using detailed kinetic mechanisms for the gas and solid phase. Furthermore, this work introduced a novel reactor type (sPFR), enabling the combined description of solid, and gas phases in one reactor to represent straight flow patterns. Detailed insights on the thermal and fluid dynamic aspects from CFD and experiments were transferred into the design of the corresponding CRN.

With these developments in CRN modeling, global as well as local characteristics of the pulverized coal combustion under oxy-fuel conditions are well captured within a multi-phase reactor network. The results show that the thermochemical state of major gaseous species can be predicted satisfactorily. Simultaneously, properties of the solids, such as burnout and release of volatiles, are consistent with experiments and CFD. A sensitivity study revealed the contributions of the gas and solid phase to the CO formation, which was under-predicted with the initial CRN. Significant improvements in the prediction of CO emissions were achieved with a sensitivity-based network design. This approach enables the analysis of CO emissions as well as minor species like NOx and SOx, demonstrating the potential of detailed kinetics in multi-phase combustion.

Future works could adapt the reactor network approach to examine solid fuel combustion processes employing biomass or metal fuels in complex burner configurations. A further enhancement of the approach in terms of repetitive engineering is an automated CRN design based on CFD data, considering local information on gas phase as well as solid phase characteristics.

Declaration of competing interest

The authors declare that they have no known competing financial interests or personal relationships that could have appeared to influence the work reported in this paper.

Data availability

Data will be made available on request.

Acknowledgments

Funded by the Hessian Ministry of Higher Education, Research, Science and the Arts - cluster project Clean Circles. Prof. Tiziano Faravelli is grateful for a related DFG Mercator Fellowship. The authors would like to thank Prof. Alberto Cuoci, Prof. Alessandro Stagni for the fruitful discussions and advice.

References

[1] World energy outlook 2022. IEA; 2022, URL https://www.iea.org/reports/world-energy-outlook-2022.
[2] Chen L, Yong SZ, Ghoniem AF. Oxy-fuel combustion of pulverized coal: Characterization, fundamentals, stabilization and CFD modeling. Prog Energy Combust Sci 2012;38(2):156–214.
[3] Li T, Farmand P, Geschwindner C, Greifenstein M, Köser J, Schumann C, Attili A, Pitsch H, Dreizler A, Böhm B. Homogeneous ignition and volatile combustion of single solid fuel particles in air and Oxy -fuel conditions. Fuel 2021;291:120101.
[4] Marek E, Świątkowski B. Experimental studies of single particle combustion in air and different Oxy -fuel atmospheres. Appl Therm Eng 2014;66(1):35–42.
[5] Schneider H, Valentiner S, Vorobiev N, Böhm B, Schiemann M, Scherer V, Kneer R, Dreizler A. Investigation on flow dynamics and temperatures of solid fuel particles in a gas-assisted Oxy -fuel combustion chamber. Fuel 2021;286:119424.
[6] Toporov D, Bocian P, Heil P, Kellermann A, Stadler H, Tschunko S, Förster M, Kneer R. Detailed investigation of a pulverized fuel swirl flame in CO2/O2 atmosphere. Combust Flame 2008;155(4):605–18.
[7] Zabrodiec D, Massmeyer A, Hees J, Hatzfeld O, Kneer R. Flow pattern and behavior of 40 kWth pulverized torrefied biomass flames under atmospheric and Oxy -fuel conditions. Renew Sustain Energy Rev 2021;138:110493.
[8] Nicolai H, Kuenne G, Knappstein R, Schneider H, Becker L, Hasse C, di Mare F, Dreizler A, Janicka J. Large eddy simulation of a laboratory-scale gas-assisted pulverized coal combustion chamber under Oxy -fuel atmospheres using tabulated chemistry. Fuel 2020;272.
[9] Nicolai H, Li T, Geschwindner C, di Mare F, Hasse C, Böhm B, Janicka J. Numerical investigation of pulverized coal particle group combustion using tabulated chemistry. Proc Combust Inst 2021;38(3):4033–41.
[10] Nicolai H, Debiagi P, Wen X, Dressler L, Massmeyer A, Janicka J, Hasse C. Flamelet LES of swirl-stabilized Oxy -fuel flames using directly coupled multi-step solid fuel kinetics. Combust Flame 2022;241:112062.
[11] Hasse C, Debiagi P, Wen X, Hildebrandt K, Vascellari M, Faravelli T. Advanced modeling approaches for CFD simulations of coal combustion and gasification. Prog Energy Combust Sci 2021;86:100938.
[12] Rieth M, Proch F, Rabaçal M, Franchetti B, Cavallo Marincola F, Kempf A. Flamelet LES of a semi-industrial pulverized coal furnace. Combust Flame 2016;173:39–56.
[13] Trespi S, Nicolai H, Debiagi P, Janicka J, Dreizler A, Hasse C, Faravelli T. Development and application of an efficient chemical reactor network model for Oxy -fuel combustion. Energy Fuels 2021;35(9):7121–32.
[14] Faravelli T, Bua L, Frassoldati A, Antifora A, Tognotti L, Ranzi E. A new procedure for predicting NOx emissions from furnaces. Comput Chem Eng 2001;25(4):613–8.
[15] Stagni A, Cuoci A, Frassoldati A, Faravelli T, Ranzi E. A fully coupled, parallel approach for the post-processing of CFD data through reactor network analysis. Comput Chem Eng 2014;60:197–212.
[16] Innocenti A, Andreini A, Bertini D, Facchini B, Motta M. Turbulent flow-field effects in a hybrid CFD-CRN model for the prediction of NOx and CO emissions in aero-engine combustors. Fuel 2018;215:853–64.
[17] Jourdan N, Neveux T, Potier O, Kanniche M, Wicks J, Nopens I, Rehman U, Le Moullec Y. Compartmental modelling in chemical engineering: A critical review. Chem Eng Sci 2019;210:115196.
[18] Haag J, Gentric C, Lemaitre C, Leclerc J-P. Modelling of chemical reactors: From systemic approach to compartmental modelling. Int J Chem React Eng 2018;16(8):20170172.
[19] Ehrhardt K, Toqan P, Jansohn P, Teare JD, Beer JM, Sybon G, Leuckel W. Modeling of nox reburning in a pilot scale furnace using detailed reaction kinetics. Combust Sci Technol 1998;131(1–6):131–46.
[20] Benedetto D, Pasini S, Falcitelli M, Marca CL, Tognotti L. NOX emission prediction from 3-D complete modelling to reactor network analysis. Combust Sci Technol 2000;153(1):279–94.
[21] Menage D, Lemaire R, Seers P. Experimental study and chemical reactor network modeling of the high heating rate devolatilization and oxidation of pulverized bituminous coals under air, Oxy gen-enriched combustion (OEC) and Oxy -fuel combustion (OFC). Fuel Process Technol 2018;177:179–93.
[22] Ishihara S, Zhang J, Ito T. Numerical calculation with detailed chemistry of effect of ammonia co-firing on NO emissions in a coal-fired boiler. Fuel 2020;266:116924.
[23] Darido J, Dhahak A, Bounaceur R, Le Dreff Lorimier C, Leyssens G, Cazier F, Genevray P, Battin-Leclerc F. Emissions from a domestic wood heating appliance: Experimental measurements and numerical study using an equivalent reactor network (ERN) approach coupled with a detailed chemical mechanism. Energy Fuels 2021;35(22):18680–98.
[24] Stark AK, Altantzis C, Bates RB, Ghoniem AF. Towards an advanced reactor network modeling framework for fluidized bed biomass gasification: Incorporating information from detailed CFD simulations. Chem Eng J 2016;303:409–24.
[25] Berkel LL, Debiagi P, Nicolai H, Amjed MA, Stagni A, Hasse C, Faravelli T. Development of a multiphase chemical reactor network method as a tool for simulating biomass gasification in fluidized beds. Fuel 2024;357:129731.

[26] Debiagi PEA, Pecchi C, Gentile G, Frassoldati A, Cuoci A, Faravelli T, Ranzi E. Extractives extend the applicability of multistep kinetic scheme of biomass pyrolysis. Energy Fuels 2015;29(10):6544–55.
[27] Sommariva S, Maffei T, Migliavacca G, Faravelli T, Ranzi E. A predictive multi-step kinetic model of coal devolatilization. Fuel 2010;89(2):318–28.
[28] Debiagi P, Ontyd C, Pielsticker S, Schiemann M, Faravelli T, Kneer R, Hasse C, Scherer V. Calibration and validation of a comprehensive kinetic model of coal conversion in inert, air and Oxy -fuel conditions using data from multiple test rigs. Fuel 2021;290:119682.
[29] Knappstein R, Kuenne G, Becker LG, di Mare F, Sadiki A, Dreizler A, Janicka J. Flamelet LES of a semi-industrial pulverized coal furnace. Flow Turbul Combust 2018;101:895–926.
[30] Senneca O, Vorobiev N, Wütscher A, Cerciello F, Heuer S, Wedler C, Span R, Schiemann M, Muhler M, Scherer V. Assessment of combustion rates of coal chars for Oxy -combustion applications. Fuel 2019;238:173–85.
[31] Cuoci A, Frassoldati A, Faravelli T, Ranzi E. OpenSMOKE++: An object-oriented framework for the numerical modeling of reactive systems with detailed kinetic mechanisms. Comput Phys Comm 2015;192:237–64.
[32] Siek JG, Lee L-Q, Lumsdaine A. The boost graph library: user guide and reference manual. Pearson Education; 2001.
[33] Becker LG, Kosaka H, Böhm B, Doost S, Knappstein R, Habermehl M, Kneer R, Janicka J, Dreizler A. Experimental investigation of flame stabilization inside the quarl of an Oxy fuel swirl burner. Fuel 2017;201:124–35.
[34] Bürkle S, Becker LG, Agizza MA, Dreizler A, Wagner S. Comparison of two measurement strategies to obtain the residence time distribution in combustion chambers using tunable diode laser absorption spectroscopy. Appl Opt 2019;58(10).
[35] Bürkle S. Laser-based investigation of gas and solid fuel combustion under Oxy -fuel atmosphere: laserbasierte untersuchung von feststoff-und gasverbrennung unter Oxy -fuel-atmosphäre. BoD – Books on Demand; 2019.
[36] Agizza MA, Bagheri G, Bürkle S, Faravelli T, Wagner S, Dreizler A. Investigation of Oxy -fuel combustion through reactor network and residence time data. Energies 2022;15(1).
[37] Maßmeyer A, Zabrodiec D, Hees J, Kreitzberg T, Hatzfeld O, Kneer R. Flame pattern analysis for 60kwth flames under conventional air-fired and Oxy -fuel conditions for two different types of coal. Fuel 2020;271:117457.
[38] Bürkle S, Becker LG, Dreizler A, Wagner S. Experimental investigation of the flue gas thermochemical composition of an Oxy -fuel swirl burner. Fuel 2018;231:61–72.
[39] Hill S, Douglas Smoot L. Modeling of nitrogen oxides formation and destruction in combustion systems. Prog Energy Combust Sci 2000;26(4):417–58.
[40] Shaddix CR, Molina A. Fundamental investigation of NOx formation during Oxy -fuel combustion of pulverized coal. Proc Combust Inst 2011;33(2):1723–30.